# TECHNICAL MEMORANDUM

X-653



## COMPARISON OF THE EFFECTIVENESS OF FLARES WITH THAT OF FINS FOR STABILIZING LOW-FINENESS-RATIO BODIES AT MACH NUMBERS FROM 0.6 TO 5.8

By Leland H. Jorgensen, J. Richard Spahr,
and William A. Hill, Jr.

Ames Research Center
Moffett Field, Calif.



NATIONAL AERONAUTICS AND SPACE ADMINISTRATION
WASHINGTON
May 1962

[redacted]

1B

~~CONFIDENTIAL~~

NATIONAL AERONAUTICS AND SPACE ADMINISTRATION

TECHNICAL MEMORANDUM X-653

# COMPARISON OF THE EFFECTIVENESS OF FLARES WITH THAT OF FINS FOR STABILIZING LOW-FINENESS-RATIO BODIES AT MACH NUMBERS FROM 0.6 TO 5.8*

By Leland H. Jorgensen, J. Richard Spahr,
and William A. Hill, Jr.

## SUMMARY

An experimental and analytical investigation has been made of the effectiveness of flares and of fins for providing aerodynamic stability of low-fineness-ratio bodies near zero angle of attack. Wind-tunnel tests were performed at Mach numbers from 0.6 to 5.8 to measure the normal force, center of pressure, and drag of bodies consisting of conical noses in combination with cylindrical midsections and finned or flared aftersections. This study included an investigation of the effects of nose bluntness, midbody length, flare angle (from $0^\circ$ to $20^\circ$), and fin leading-edge bluntness.

The results showed that for the same plan-form area, flares were more effective than fins, but for the same drag, fins were more effective than flares. Flow separation, which occurred ahead of a flare at certain Mach numbers, resulted in an increase in the stabilizing effectiveness of the flare and a decrease in the drag. However, flow separation led to large undesirable shifts in the center of pressure. Blunt fins were found to be more effective than sharp fins, with the vertical as well as the horizontal fins contributing to the effectiveness.

Comparisons of the analytical with the experimental results indicated that the analytical method employed gave good estimates of the stabilizing effectiveness of both fins and flares throughout the supersonic Mach number range.

*Title, Unclassified

~~CONFIDENTIAL~~

## INTRODUCTION

The relative effectiveness of flares as compared with fins for stabilizing bodies of low fineness ratio is of interest in the design of ballistic and atmospheric entry vehicles. Although many investigations have been made of the effectiveness of flares for stabilizing bodies (e.g., refs. 1 through 10), there is a need for direct comparisons of flare and fin effectiveness over a wide Mach number range. Accordingly, an investigation was conducted to determine the stability and drag of several flared and finned bodies at Mach numbers from 0.6 to 5.8. Models consisting of conical noses with cylindrical midsections and finned or flared aftersections were tested. This study included investigation of the effects of flare angle (from $0^\circ$ to $20^\circ$) and of nose and fin bluntness. The range of flare angles chosen enabled normal-force and stability comparisons of finned and flared models to be made on the basis of either specified equal plan-form area or equal drag. Both experimental and analytical comparisons have been made, and the purpose of this report is to discuss these comparisons.

A 5 7 5

## NOTATION

$A$ cross-sectional area of cylindrical portion of body

$a$ fin semispan measured from surface of cylindrical portion of body

$C_D$ drag coefficient (exclusive of base drag) at zero angle of attack

$C_{m_\alpha}$ pitching-moment-curve slope referred to the moment centers shown in figures 8, 9, and 12,

$$\frac{d}{d\alpha}\left(\frac{\text{pitching moment}}{q_\infty A d}\right)$$

$C_{N_\alpha}$ normal-force-curve slope, $\frac{d}{d\alpha}\left(\frac{\text{normal force}}{q_\infty A}\right)$

$C_{p_{stag}}$ stagnation pressure coefficient, $\frac{p_{stag} - p_\infty}{q_\infty}$

$d$ diameter of cylindrical portion of body

$d'$ body base diameter

| | |
|---|---|
| $d_w$ | trip wire diameter |
| E | complete elliptic integral of second kind |
| K | ratio of normal-force component to normal force of fin alone |
| $l$ | length |
| M | free-stream Mach number |
| $p_{stag}$ | stagnation pressure |
| $p_\infty$ | free-stream static pressure |
| $q_\infty$ | free-stream dynamic pressure |
| R | Reynolds number based on d |
| r | radius of fin leading edge |
| $r_S$ | radius of spherical portion of nose |
| $x_{cp}$ | center of pressure measured rearward from nose-cylinder juncture |
| $x'_{cp}$ | center of pressure measured rearward from moment centers shown in figures 8, 9, and 12 |
| $\alpha$ | angle of attack, deg |
| $\beta$ | $\sqrt{M^2 - 1}$ |
| $\delta$ | half-angle, deg |

A 5 7 5

## Subscripts

| | |
|---|---|
| A | aftersection |
| B(W) | body in presence of fins |
| C | unblunted cone |
| cy | cylinder |
| F | fins |
| Fl | flare |

N nose

S spherical portion of nose

W(B) fins in presence of body

## EXPERIMENTAL CONSIDERATIONS

### Wind Tunnels

The experimental investigation was conducted in the Ames 2- by 2-Foot Transonic Wind Tunnel and the 1- by 3-Foot Supersonic Wind Tunnel. The 2- by 2-foot tunnel is of the closed-circuit, variable-pressure type. It has a flexible-plate nozzle and a perforated test section which permits continuous choke-free operation at Mach numbers up to 1.4. The 1- by 3-foot tunnel is also a closed-circuit, variable-pressure type and has a flexible-plate nozzle that provides a variation of Mach number from about 1.4 to 6. In these tunnels the Reynolds number is changed by varying the total pressure within the approximate limits of 1/5 of an atmosphere to 4 atmospheres.



The water content of the air in the tunnels is maintained at less than 0.0003 pound of water per pound of dry air. Consequently, any effect of humidity on the flow is negligible.

### Models

In order to determine the stabilizing effectiveness of flares and fins, models consisting of bodies with and without flared and finned aftersections were tested. Sketches and designations of the models are shown in figure 1 in three groupings: nose shapes and bodies (fig. 1(a)), bodies with flares (fig. 1(b)), and bodies with cruciform fins (fig. 1(c)). In addition, the sizes and positions of wire rings that were placed on the body noses to trip the boundary layer are shown in figure 1(d). Two nose shapes were used: one, a sharp cone of $14^{\circ}2'$ semiapex angle (designated $N_S$), and the other, a spherically blunted cone ($2r_S/d = 0.50$) with the same cone angle (designated $N_B$). These nose pieces were constructed for testing both separately and with cylindrical bodies of 2 and 3.37 diameters in length (designated C and $C_L$, respectively). The cylindrical bodies were constructed so that flared or finned aftersections could be attached. All of the flared aftersections were of equal length (1.373 diameters) but with flare angles of $0^{\circ}$, $10^{\circ}$, and $20^{\circ}$ (fig. 1(b)). The finned aftersections were of the same length and plan form as the $20^{\circ}$ flared aftersection. As noted in figure 1(c), cruciform fins with all sharp or all blunt leading edges and combinations of sharp and blunt

leading edges were employed. In addition, a model with blunt fins superimposed on a 10° flare was tested. All models were sting mounted from the rear with a strain-gage balance positioned inside each model. Photographs of typical flared and finned models mounted in the 1- by 3-foot supersonic wind tunnel are shown in figure 2.

## Tests

A 5 7 5 Tests were made to determine the normal-force-curve slope, center of pressure, drag, and boundary-layer-flow characteristics of the models at zero angle of attack for various Mach numbers. The test Mach numbers and Reynolds numbers based on body diameter are summarized in the following table:

| M | $R \times 10^{-6}$ | Tunnel |
|---|---|---|
| 0.60 to 1.40 | 0.38 | 2- by 2-foot |
| 1.37 to 4.06 | .49 | 1- by 3-foot |
| 5.11 | .35 | 1- by 3-foot |
| 5.82 | .18 | 1- by 3-foot |

To determine accurately the normal-force-curve slopes and centers of pressure at zero angle of attack, the models were tested at half degree increments throughout the $\alpha$ range from -4° to +4°. The blunt-nosed bodies alone and in combination with the flared and finned aftersections were tested throughout the entire Mach number range (M = 0.60 to 5.82). The sharp-nosed models and the models with combined sharp and blunt fins ($N_BCF_{B_V}S_H$ and $N_BCF_{B_H}S_V$) were tested only at selected supersonic Mach numbers. All of the models were tested with wire rings mounted on their noses in an effort to trip the boundary-layer flow (fig. 1(d)). The blunt-nosed model with the 20° flare ($N_BCFl_{20}$) was also tested without any rings at Mach numbers from 2.94 to 5.81. For all tests the shadowgraph technique was employed to observe model boundary-layer flow.

## Reduction and Precision of Data

All of the force and moment data have been reduced to coefficient form. From plots of normal-force coefficient and pitching-moment coefficient versus angle of attack, values of $C_{N_\alpha}$ and $C_{m_\alpha}$ were determined, and center-of-pressure positions ($x_{cp}/d$) were computed. The measured base pressures were used to compute the base drag which was subtracted from the total drag measurements, so that the drag coefficients presented are for forces ahead of the body base.

The precision of the final data is affected by uncertainties in the measurement of the forces and moments, and in the determination of the stream static and dynamic pressures used in reducing the forces and moments to coefficient form. These individual uncertainties led to the following estimated uncertainties:

| | |
|---|---|
| $C_{N_\alpha}$ ±0.0015 per deg | $\alpha$ ±0.1° |
| $x_{cp}/d$ ±0.04 | M ±0.01 for $M \leq 2.94$ |
| $C_D$ ±0.015 | M ±0.03 for $M > 2.94$ |

## RESULTS AND DISCUSSION

For all the models tested, experimental values of $C_{N_\alpha}$, $x_{cp}/d$, and $C_D$ as functions of Mach number are presented in figures 3 through 6. Results for the nose shapes and bodies are given in figure 3, while those for the bodies with flares and for the bodies with fins are given in figures 4 and 5, respectively. In figure 6 results are compared for the flared and finned bodies of equal plan-form area. Data for the models having boundary-layer trip rings are designated by unflagged symbols, whereas results for the models without trip rings are designated by flagged symbols. Representative shadowgraphs are shown in figure 7. Reference is made to these figures in the following discussion which is divided into two major sections: (1) comparison of experimental effectiveness of flares and fins and (2) comparison of computed with experimental results.

### Comparison of Experimental Effectiveness of Flares and Fins

Flared and finned models of equal plan-form area.- Throughout the Mach number range, the results clearly show that flares are more effective than fins of equal plan-form area. For example, in figure 6 it is seen that the values of $C_{N_\alpha}$ (fig. 6(a)) for the flared models were higher at supersonic speeds than those for comparable finned models, and the centers of pressure (fig. 6(b)) were more rearward. As a result, the flare provided considerably more stability than the fins, especially at the higher Mach numbers. The gains in effectiveness of the flared over the finned models were, of course, accompanied by much greater drag for the flared models (fig. 6(c)).

It is important to note here that some of the aerodynamic characteristics for the 20° flared models were greatly influenced by flow separation ahead of the flare. The occurrence of flow separation was

detected from shadowgraphs, some of which are reproduced in figure 7. It is seen in figure 7(a) that a large region of turbulent-flow separation occurred in the vicinity of the flare-cylinder juncture at $M = 1.20$. This separation resulted in the sharp rise in $C_{N_\alpha}$ shown in figure 6(a) at Mach numbers from about 1.1 to 1.2. The decrease in $C_{N_\alpha}$ as the Mach number was increased from about 1.2 to 1.4 was probably due to a reduction in the extent of the turbulent separation, as evidenced in the shadowgraph at $M = 1.37$ (fig. 7(b)). At higher supersonic Mach numbers, effects of laminar flow separation appeared in the measured data. At the test Mach numbers of 2.94 and 4.06, removal of the nose-mounted transition rings (shown in fig. 1(d)) resulted in laminar flow with separation beginning well in front of the flare. (Compare shadowgraph showing turbulent flow, fig. 7(c), with shadowgraph showing laminar flow separation, fig. 7(d).) The large increase in $C_{N_\alpha}$ for the model with laminar separated flow over that for the same model with turbulent attached flow is evident in figure 6(a). At the test Mach numbers greater than 4.05, the transition rings were completely ineffective, laminar flow separation occurring with the rings attached as well as removed. Flow separation (whether laminar or turbulent) not only resulted in a higher $C_{N_\alpha}$ but also in a more rearward center of pressure and a reduced drag. Thus, the effects of flow separation were beneficial at a particular Mach number; however, the large shift in center of pressure when the flow changed from attached to separated was undesirable.

A 5 7 5

Although blunted fins were used for the fin and flare comparisons in figure 6, the same general conclusions were reached when results for the flared model, $N_BCFl_{20}$, were compared with those for the comparable sharp-finned model, $N_BCF_S$. In fact, as shown in figure 5, blunting of either horizontal or vertical fins or both was beneficial in increasing effectiveness, so that the advantage of flares over sharp fins was even greater than over blunted fins.

Direct comparisons of the stabilizing effectiveness of fins and flares have been made by subtracting the short-forebody, $N_BC$, results (fig. 3) from the results for the flared and finned models (figs. 4 and 5). The ratios $C_{N_\alpha,Fl}/C_{N_\alpha,F}$, $C_{m_\alpha,Fl}/C_{m_\alpha,F}$, and $x'_{cp,Fl}/x'_{cp,F}$ have been determined and are presented as a function of Mach number in figure 8. For the $C_{m_\alpha}$ comparisons, the center of moments was taken at the fin-cylinder or flare-cylinder juncture (1.37 cylinder diameters forward of the base). The center-of-pressure positions, $x'_{cp}$, were referenced from this juncture as indicated in the sketch of figure 8. This figure clearly demonstrates the increasing stability advantage of flares over fins as Mach number was increased. It also shows the great increase in stability attributable to flow separation.

Flared and finned models of equal drag.- For certain applications, comparisons of the effectiveness of flares with that of fins of equal drag may be of greatest interest. Although no tests were made of a flared model having the same drag as the 20° blunt-finned model, $N_BCF_B$, it was found by interpolation of the drag results for the flared models that the flare angle for such a model would be about 7° at the supersonic Mach numbers considered. Values of $C_{N_\alpha}$ and $x_{cp}/d$ for this model were then determined by interpolation. As for the models of equal plan-form area, the results for the forebody alone were subtracted from those for the total model and the ratios $C_{N_{\alpha,F}}/C_{N_{\alpha,Fl}}$, $C_{m_{\alpha,F}}/C_{m_{\alpha,Fl}}$, and $x'_{cp,F}/x'_{cp,Fl}$ were determined. These ratios, presented in figure 9, clearly show the greater effectiveness of the fins. However, it is important to note that the advantage of fins over flares decreased with increasing Mach number.

## Comparisons of Computed With Experimental Results

Comparisons of computed with experimental results (figs. 10 and 11) indicate that for models without flow separation, the aerodynamic characteristics can be predicted reasonably well by the methods outlined in the appendix. No attempt was made to predict the conditions for flow separation or the effects of separation on the forces and moments. As seen in figure 10 for a model with a 20° flare ($N_BCFl_{20}$), flow separation in front of the flare resulted in values of $C_{N_\alpha}$ much greater than computed, and centers of pressure much more rearward. For the models with attached flow the calculated curves were determined both with and without the inclusion of experimental lift from the cylindrical body. In the calculative procedure outlined in the appendix, it was assumed that there was no lift from the body cylinder. However, from the experimental results for the nose and for the nose with body (shown in fig. 3), it was found that the cylindrical portion of the body was contributing to the lift. In figures 10 and 11, the calculated curves with the experimental lift of the cylindrical body included are generally in better agreement with experiment than those without it.

Comparisons of computed with experimental stabilizing effectiveness of fins relative to flares have been made and are presented in figure 12. These comparisons are presented for the specified conditions of equal plan-form area (fig. 12(a)) and equal drag (fig. 12(b)). As for the experimental results previously presented in figures 8 and 9, the comparisons are general in that the forebody contribution to the aerodynamic characteristics was not included. On the basis of equal plan-form area (fig. 12(a)), the increase in superiority of flares over fins as Mach number was increased was closely predicted except when flow separation occurred. For specified equal drag (fig. 12(b)), the decrease with Mach number of the advantage of fins over flares was only approximated by theory. However, the theoretical and experimental trends with

Mach number indicate that there may be little or no advantage of fins over flares at Mach numbers above about 6.

## CONCLUSIONS

Wind-tunnel tests and theoretical calculations have been made to compare the effectiveness of flares with that of fins for stabilizing low-fineness-ratio bodies near zero angle of attack over the Mach number range of 0.6 to 5.8. On the basis of this investigation, the following conclusions have been drawn:

A 5 7 5

1. Flares provided more stability but also more drag than fins of the same plan-form area. With increase in Mach number, the stability advantage of flares over fins increased and the drag disadvantage diminished.

2. Fins provided more stability than a flare having the same drag. With increase in Mach number, however, the stability advantage of fins decreased.

3. Flow separation, which occurred ahead of a flare at some Mach numbers, caused an increase in the stabilizing effectiveness and a decrease in the drag of the flare, but this effect led to large undesirable shifts in the center of pressure.

4. Blunt fins gave more longitudinal stability than sharp fins of the same plan area, with the vertical as well as the horizontal fins contributing to the stabilizing effectiveness.

5. The aerodynamic characteristics contributed by the fins or flares were virtually unaffected by changes in nose bluntness or body length.

6. Analytical methods provided good estimates of the fin and flare effectiveness at supersonic Mach numbers.

Ames Research Center
National Aeronautics and Space Administration
Moffett Field, Calif., Mar. 19, 1962

# APPENDIX

## FORMULAS FOR PREDICTING THE AERODYNAMIC CHARACTERISTICS OF FLARED OR FINNED BODIES

General analytical expressions have been derived for the calculation of $C_{N_\alpha}$, $C_{m_\alpha}$, and $C_D$ for the component parts of a flared or finned body at zero angle of attack. The aerodynamic characteristics for the composite body, illustrated in sketch (a), were taken as the sum of the characteristics for the parts. Formulas for computing the characteristics for

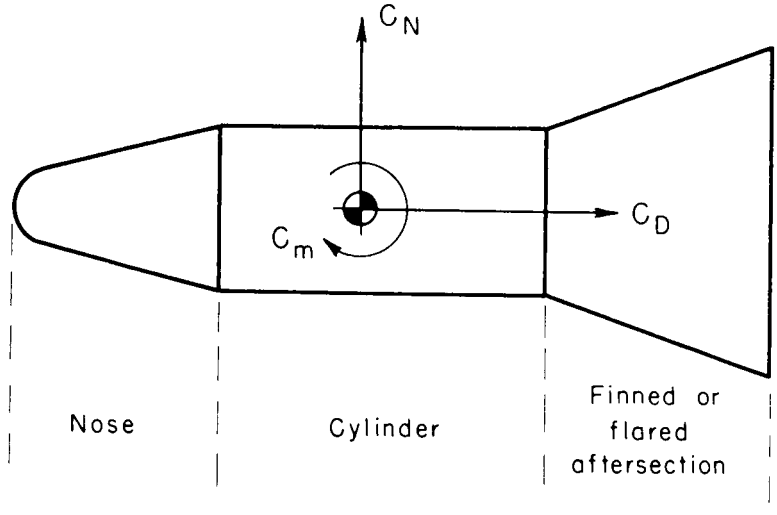


Sketch (a)

the component parts are presented in the following sections. No formulas are presented for the cylindrical portion of the body, since the theoretical values of $C_{N_\alpha}$, $C_{m_\alpha}$, and $C_D$ (exclusive of skin-friction drag) are all zero.

## $C_{N_\alpha}$ AND $C_{m_\alpha}$ AT ZERO ANGLE OF ATTACK

### Body Nose

For a spherically blunted cone (sketch (b)), the expressions for $C_{N_\alpha}$ and $C_{m_\alpha}$ in terms of $C_{N_\alpha,S}$ for a spherical segment and $C_{N_\alpha,C}$ for a sharp-nosed cone are

$$C_{N_{\alpha,N}} = \left(\frac{2r_S}{d}\right)^2 C_{N_{\alpha,S}} + \left[1 - \left(\frac{2r_S \cos \delta_N}{d}\right)^2\right] C_{N_{\alpha,C}} \quad (1)$$

$$C_{m_{\alpha,N}} = -\frac{1}{2 \sin \delta_N}\left(\frac{2r_S}{d}\right)^3 C_{N_{\alpha,S}} - \frac{2}{3 \sin 2\delta_N}\left[1 - \left(\frac{2r_S \cos \delta_N}{d}\right)^3\right] C_{N_{\alpha,C}} + \frac{x_N}{d} C_{N_{\alpha,N}} \quad (2)$$

A 5 7 5

where $C_{N_{\alpha,N}}$ and $C_{m_{\alpha,N}}$ are based on the cylinder cross-sectional area, and the reference length for $C_{m_{\alpha,N}}$ is the cylinder diameter d. In the derivation of equation (2), the center of pressure of the spherical

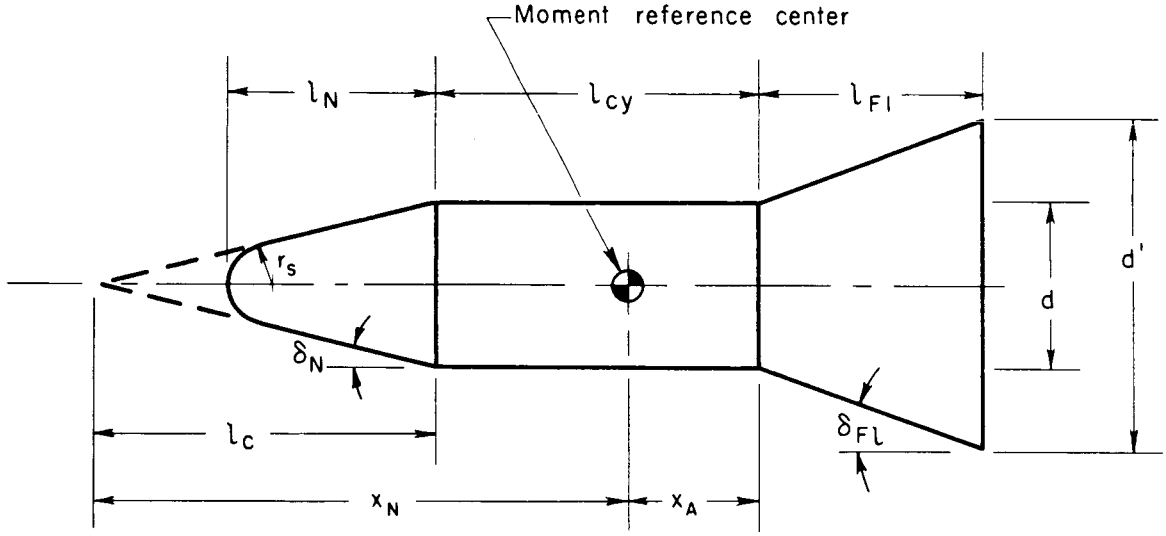


Sketch (b)

nose was taken as the center of the sphere, and the center of pressure of the nose cone without blunting was assumed to be at $2/3 \cos^2\delta_N$ of its length from the imaginary vertex. The quantity $C_{N_{\alpha,S}}$ was obtained from the modified Newtonian relationship for a spherical segment

$$C_{N_{\alpha,S}} = \frac{1}{2} C_{p_{stag}} \cos^4 \delta_N \quad (3)$$

For the calculations of this report, $C_{p_{stag}}$ was taken as 1.8. Theoretical values of $C_{N_{\alpha,C}}$ for an unblunted cone with the same $\delta_N$ as the blunted conical nose were obtained from chart 8 of reference 11.

Flared Aftersection

For a conical flared aftersection (sketch (b)), the formulas are

$$C_{N_{\alpha,Fl}} = \left[ \left( \frac{d'}{d} \right)^2 - 1 \right] C_{N_{\alpha,C}} \tag{4}$$

$$C_{m_{\alpha,Fl}} = \frac{1}{2 \tan \delta_{Fl}} \left\{ \left[ \left( \frac{d'}{d} \right)^2 - 1 \right] - \frac{2 \left[ \left( \frac{d'}{d} \right)^3 - 1 \right]}{3 \cos^2 \delta_{Fl}} \right\} C_{N_{\alpha,C}} - \frac{x_A}{d} C_{N_{\alpha,Fl}} \tag{5}$$

Finned Aftersection

For an aftersection consisting of a circular cylinder in combination with thin fins having sharp leading edges (sketch (c) with b vanishingly small), the formulas are

$$C_{N_{\alpha,F}} = K \frac{a l_F}{\frac{\pi}{4} d^2} C_{N_{\alpha,W}} \tag{6}$$

$$C_{m_{\alpha,F}} = - \left( \frac{2}{3} \frac{l_F}{d} + \frac{x_A}{d} \right) K \frac{a l_F}{\frac{\pi}{4} d^2} C_{N_{\alpha,W}} \tag{7}$$

where $K$ is the sum of the interference factors $K_{W(B)}$ and $K_{B(W)}$ given in figures 2 and 5 of reference 12 and $C_{N_{\alpha,W}}$ linearized wing theory (ref. 13)

$$\left.\begin{aligned} C_{N_{\alpha,W}} &= 2\pi \tan \delta_F \left[ \frac{1}{E \left( \sqrt{1 - \beta^2 \tan^2 \delta_F} \right)} \right] ; \qquad \beta \tan \delta_F \leq 1 \\ C_{N_{\alpha,W}} &= \frac{4}{\beta} ; \qquad \beta \tan \delta_F \geq 1 \end{aligned}\right\} \tag{8}$$

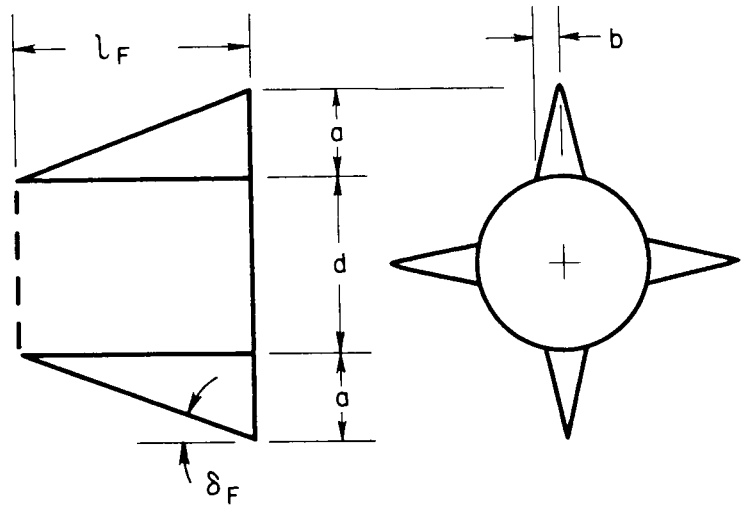


Aftersection with sharp fins

Sketch (c)

For an aftersection with blunt leading-edged fins (sketch (d)), the additional $C_{N_{\alpha,F}}$ and $C_{m_{\alpha,F}}$ caused by bluntness of the two vertical fins

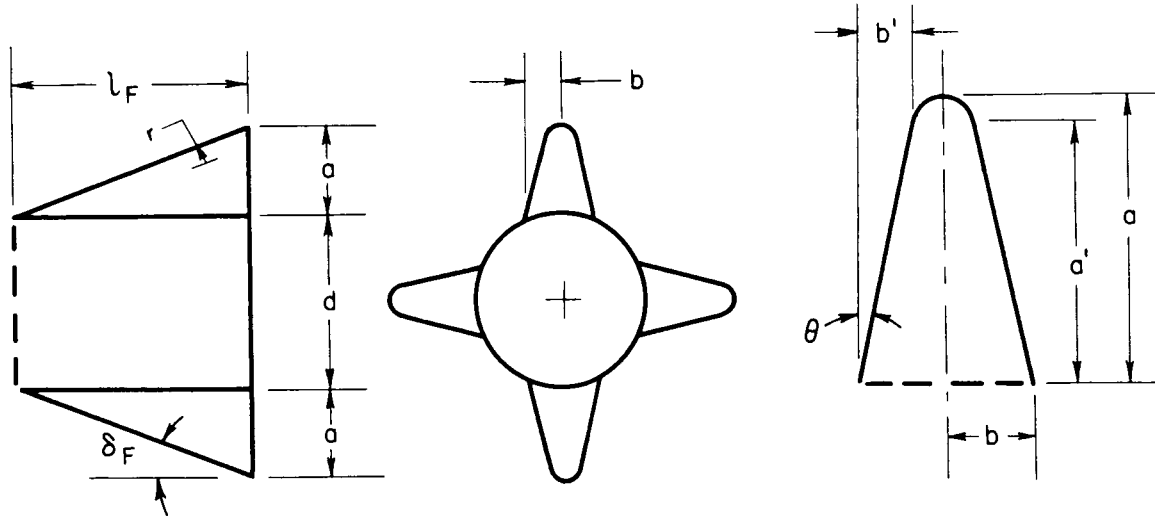


Aftersection with blunt fins

Rear view of blunt fin

Sketch (d)

were derived by the use of modified Newtonian theory. The derived expressions are

$$\Delta C_{N_{\alpha,F}} = 32 \frac{ar}{\pi d^2} \cos^2\delta_F \left(\cos\theta' - \frac{1}{3}\cos^3\theta'\right) C_{p_{stag}} \tag{9}$$

$$\Delta C_{m_{\alpha,F}} = -\left(\frac{x_A}{d} + \frac{a}{2d \tan\delta_F}\right) \Delta C_{N_{\alpha,F}} \tag{10}$$

where $\theta' = \tan^{-1}\left(\frac{\tan\theta}{\cos\delta_F}\right)$

The predicted effects on $C_{N_{\alpha,F}}$ and $C_{m_{\alpha,F}}$ of leading-edge bluntness of the horizontal fins of the present investigation were found to be negligible.

A 5 7 5

## $C_D$ AT ZERO ANGLE OF ATTACK

The drag coefficient for the complete model configuration was assumed to be equal to the sum of the drag coefficients of the component parts, with base drag coefficient omitted. For each component the drag coefficient was taken as the sum of the pressure drag and skin-friction drag coefficients. Since the boundary-layer flow over the models was believed to be essentially turbulent, the skin-friction drag coefficients were computed by the T' method, the details of which are clearly given in reference 14. The formulas which follow are for pressure drag only and apply to the general configuration in sketch (a).

### Body Nose

For the spherically blunted conical nose (sketch (b)), the drag coefficient was computed from

$$C_{D_N} = \left(\frac{2r_S}{d}\right)^2 C_{D_S} + \left[1 - \left(\frac{2r_S \cos\delta_N}{d}\right)^2\right] C_{D_C} \tag{11}$$

where $C_{D_S}$ was the drag coefficient of the spherical tip of radius $r_S$, and $C_{D_C}$ was the drag coefficient of the unblunted cone of half-angle $\delta_N$. The drag coefficient of the spherical tip $C_{D_S}$ was obtained from the modified Newtonian relationship

$$C_{D_S} = \frac{1}{2} C_{p_{stag}} (1 - \sin^4\delta_N) \tag{12}$$

For the calculations of this report, $C_{p_{stag}}$ was taken as 1.8. The drag coefficient of the unblunted cone $C_{D_C}$ was assumed to be that given by Taylor-Maccoll theory, and values of $C_{D_C}$ were obtained from chart 6 in reference 11.

## Flared Aftersection

For the flared aftersection (sketch (b)), the drag coefficient was computed from

$$C_{D_{Fl}} = \left[\left(\frac{d'}{d}\right)^2 - 1\right] C_{D_C} \tag{13}$$

where $C_{D_C}$ was the drag coefficient of the cone of diameter $d'$ and half-angles $\delta_{Fl}$. As for the conical portion of the nose, values of $C_{D_C}$ were obtained from chart 6 in reference 11.

## Finned Aftersection

Modified Newtonian theory (with $C_{p_{stag}} = 1.8$) was applied to obtain the drag coefficients for the sharp- and blunt-finned aftersections. For the sharp-finned aftersection indicated in sketch (c), the drag coefficient was estimated from

$$C_{D_F} = \frac{16\, C_{p_{stag}}}{\left[\left(\frac{l_F}{a}\right)^2 + \left(\frac{l_F}{b}\right)^2 + 1\right]} \frac{ab}{\pi d^2} \tag{14}$$

For the aftersection with the blunt leading-edged fins (sketch (d)), the drag of the rounded leading edges was added to that of the side wedges to give the expression

$$C_{D_F} = \frac{32\, C_{p_{stag}}\, ar \sin^2\delta_F}{\pi d^2}\left(\cos\theta' - \frac{\cos^3\theta'}{3}\right) + \frac{16\, C_{p_{stag}}}{\left[\left(\frac{l_{F'}}{a'}\right)^2 + \left(\frac{l_{F'}}{b'}\right)^2 + 1\right]} \frac{a'b'}{\pi d^2} \tag{15}$$

where

$$l_F' \approx \left[ a - \frac{r}{\cos \delta_F} (1 - \sin \theta) \right] \cot \delta_F$$

$$a' = a - \frac{r}{\cos \delta_F} (1 - \sin \theta)$$

$$b' = b - \frac{r}{\cos \delta_F} \cos \theta$$

$$\theta' = \tan^{-1} \left( \frac{\tan \theta}{\cos \delta_F} \right)$$

A 5 7 5

## USE OF THE FORMULAS FOR HYPERSONIC MACH NUMBERS

At hypersonic Mach numbers (probably above about 6) the formulas for the flared and finned aftersections should be multiplied by the ratio of the local to the free-stream dynamic pressure. Also, the values of $C_{N_{\alpha,C}}$, $C_{N_{\alpha,W}}$, $C_{D_C}$, and $C_{p_{stag}}$ used in the formulas should be determined for the local instead of the free-stream Mach number. If the bow shock-wave position is known, local flow conditions can be estimated by the method of reference 15. For the present investigation, however, free-stream flow conditions were assumed in all of the calculations.

## REFERENCES


1. Kehlet, Alan B.: Some Effects of Reynolds Number on the Stability of a Series of Flared-Body and Blunted-Cone Models at Mach Numbers from 1.62 to 6.86. NACA RM L57J29, 1958.

2. Dennis, David H.: The Effects of Boundary-Layer Separation Over Bodies of Revolution With Conical Tail. NACA RM A57I30, 1957.

3. Eggers, A. J., Jr., and Syvertson, Clarence A.: Experimental Investigation of a Body Flare for Obtaining Pitch Stability and a Body Flap for Obtaining Pitch Control in Hypersonic Flight. NACA RM A54J13, 1955.

4. Knechtel, Earl D., Treon, Stuart L., and Wakefield, Roy M.: Transonic Static Aerodynamic Characteristics of a Blunt Cone-Cylinder Body With Flared Afterbody or Blunt Cruciform Fins. NASA TM X-40, 1959.

5. Wakefield, Roy M., Knechtel, Earl D., and Treon, Stuart L.: Transonic Static Aerodynamic Characteristics of a Blunt Cone-Cylinder Body With Flared Afterbodies of Various Angles and Base Areas. NASA TM X-106, 1959.

6. Knechtel, Earl D., Wakefield, Roy M., and Treon, Stuart L.: Transonic Static Aerodynamic Characteristics of a Low-Fineness-Ratio Body of Revolution Having a Blunt Ellipsoidal Nose and Flared Afterbodies of Various Angles and Base Areas. NASA TM X-113, 1960.

7. Treon, Stuart L., Wakefield, Roy M., and Knechtel, Earl D.: Effects of Nose Shape and Afterbody Flare on the Transonic Characteristics of a Low-Fineness-Ratio Body of Revolution. NASA TM X-164, 1960.

8. Wakefield, Roy M., Treon, Stuart L., and Knechtel, Earl D.: Effects of Centerbody Length and Nose Shape on the Transonic Characteristics of Low-Fineness-Ratio Bodies of Revolution With a Flared Afterbody. NASA TM X-366, 1960.

9. Treon, Stuart L.: Effects of Nose Cone Angle on the Transonic Aerodynamic Characteristics of a Blunt Cone-Cylinder Body Having a Cylindrical, Flared, or Blunt-Finned Afterbody. NASA TM X-582, 1961.

10. Reese, David E., Jr., and Wehrend, William R., Jr.: An Investigation of the Static and Dynamic Aerodynamic Characteristics of a Series of Blunt-Nosed Cylinder-Flare Models at Mach Numbers From 0.65 to 2.20. NASA TM X-110, 1960.

11. Ames Research Staff: Equations, Tables, and Charts for Compressible Flow. NACA Rep. 1135, 1953.

12. Pitts, William C., Nielsen, Jack N., and Kaattari, George E.: Lift and Center of Pressure of Wing-Body-Tail Combinations at Subsonic, Transonic, and Supersonic Speeds. NACA Rep. 1307, 1957.

13. Puckett, A. E., and Stewart, H. J.: Aerodynamic Performance of Delta Wings at Supersonic Speeds. Jour. Aero. Sci., vol. 14, no. 10, Oct. 1947, pp. 567-578.

14. Shapiro, A. H.: The Dynamics and Thermodynamics of Compressible Fluid Flow. Vol. II, chs. 26 and 27, The Ronald Press Co., New York, 1954.

15. Seiff, Alvin, and Whiting, Ellis E.: Calculation of Flow Fields From Bow-Wave Profiles for the Downstream Region of Blunt-Nosed Circular Cylinders in Axial Hypersonic Flight. NASA TN D-1147, 1961.

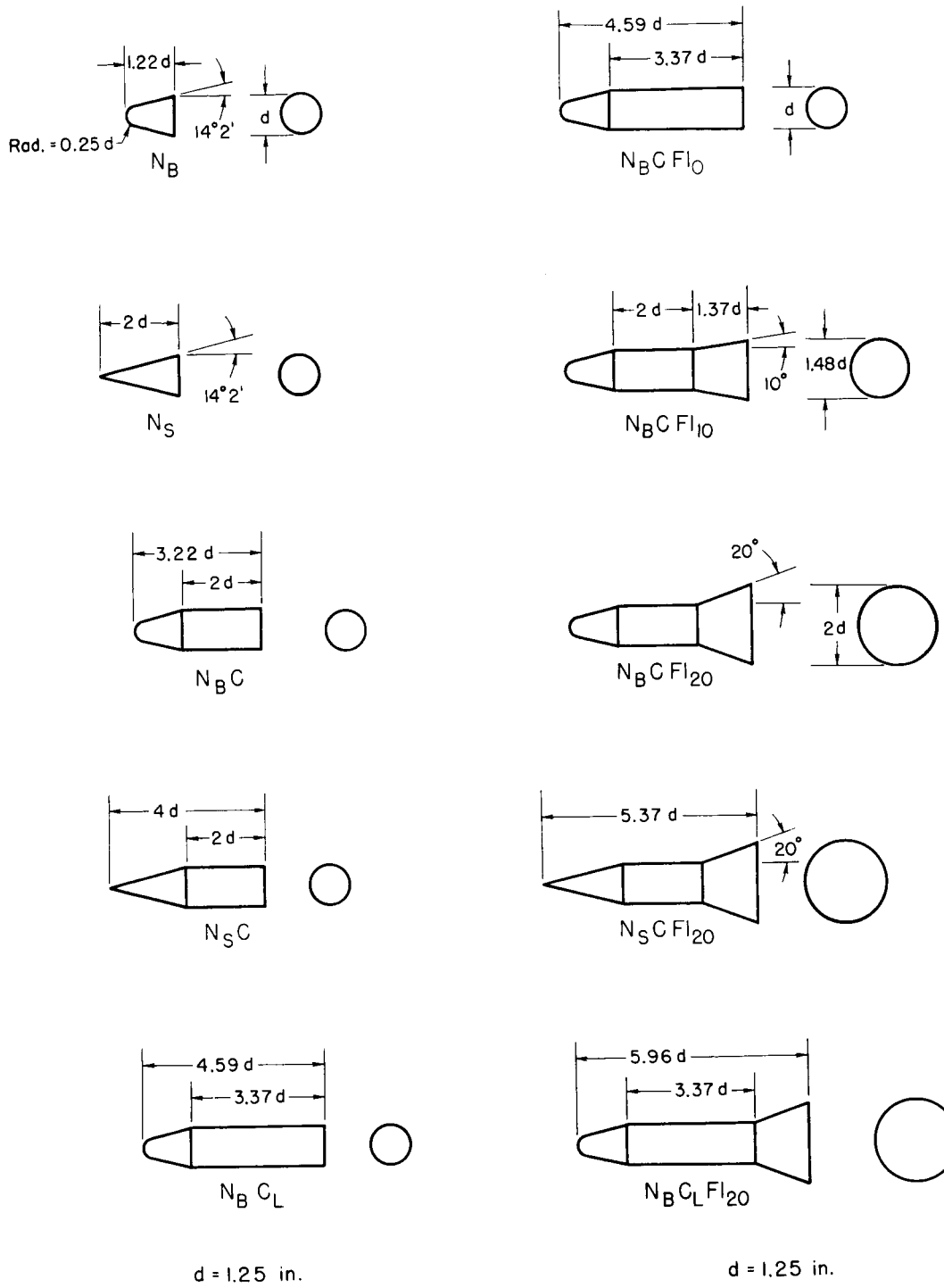


(a) Nose shapes and bodies.

(b) Bodies with flares.

Figure 1.- Models tested.

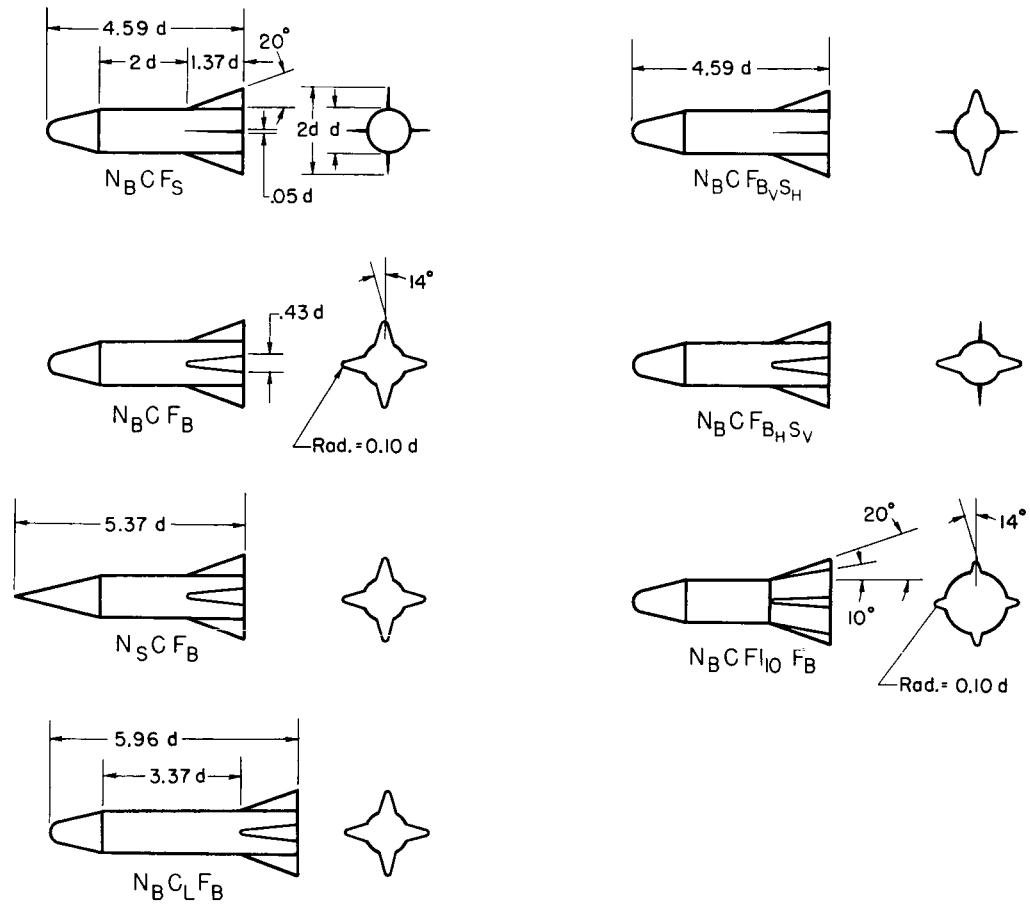


d = 1.25 in.

(c) Bodies with fins.

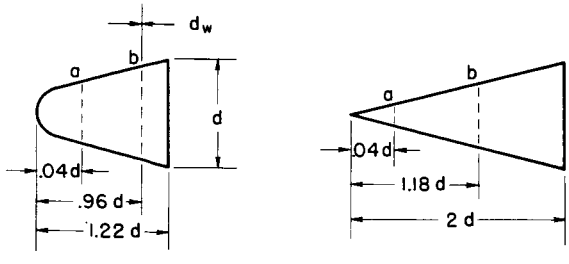


| M | Wind tunnel | Rings used | $d_w$ in. |
|---|---|---|---|
| 0.60 to 1.40 | 2 x 2 | a | 0.008 |
| 1.37 to 2.94 | 1 x 3 | a | .014 |
| 4.06 to 5.82 | 1 x 3 | a and b | .020 |

d = 1.25 in.

(d) Sizes and positions of boundary-layer trip rings.

Figure 1.- Concluded.

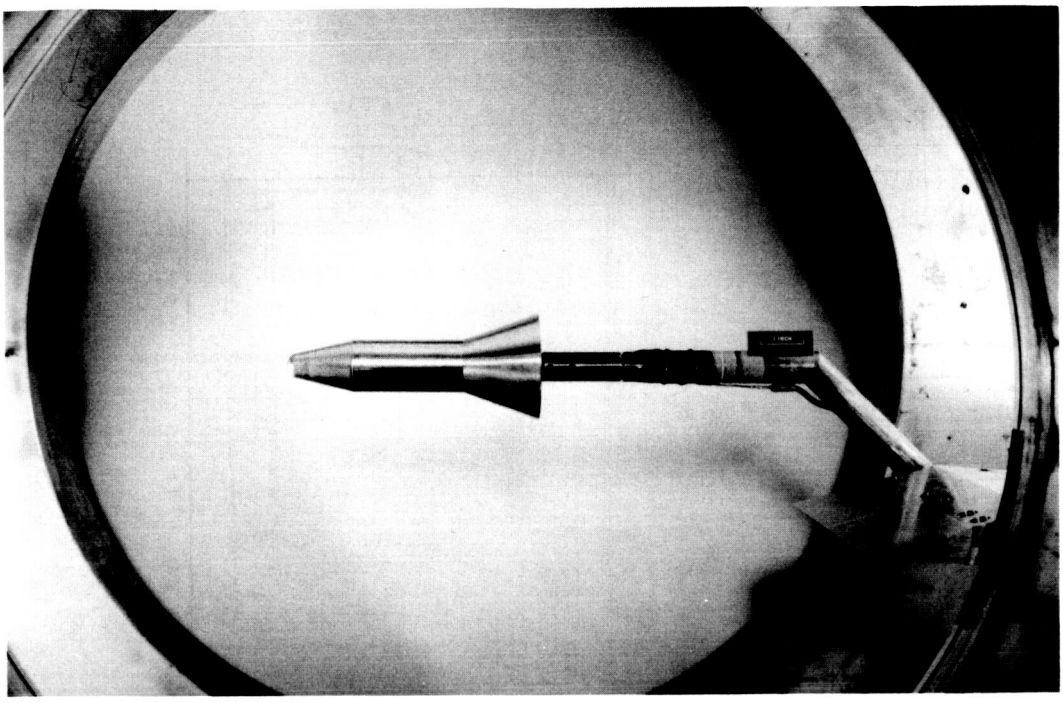

A-26685

(a) Flared model, $N_BCFl_{20}$.

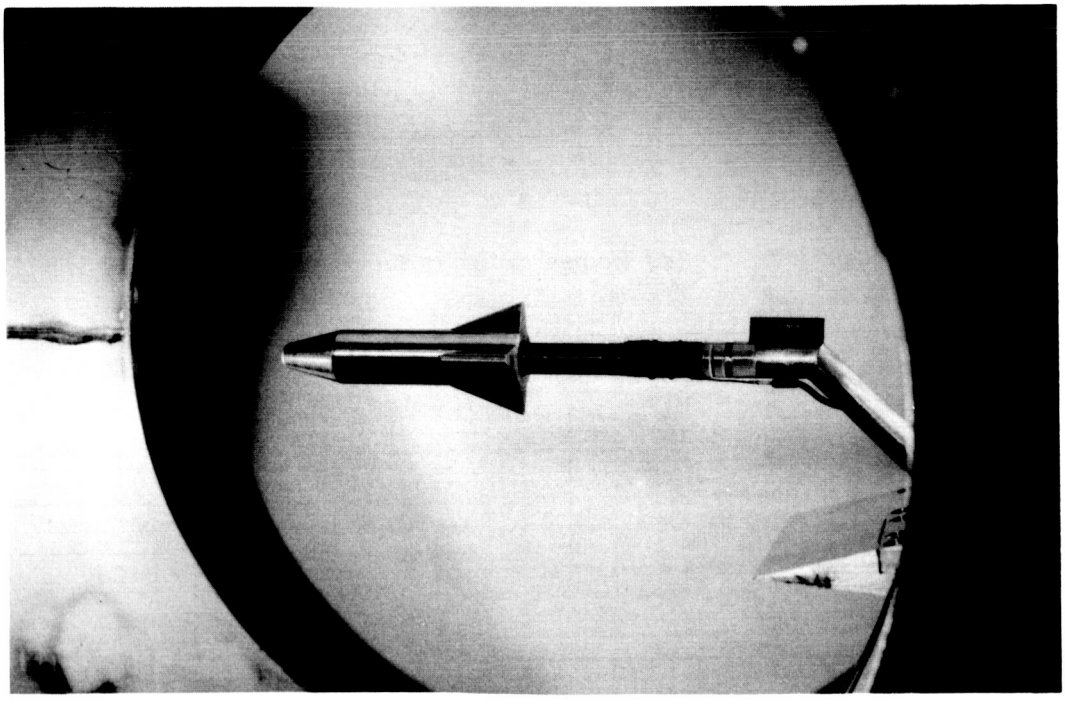

A-26686

(b) Finned model, $N_BCF_B$.

Figure 2.- Typical flared and finned models mounted in the Ames 1- by 3-Foot Supersonic Wind Tunnel.

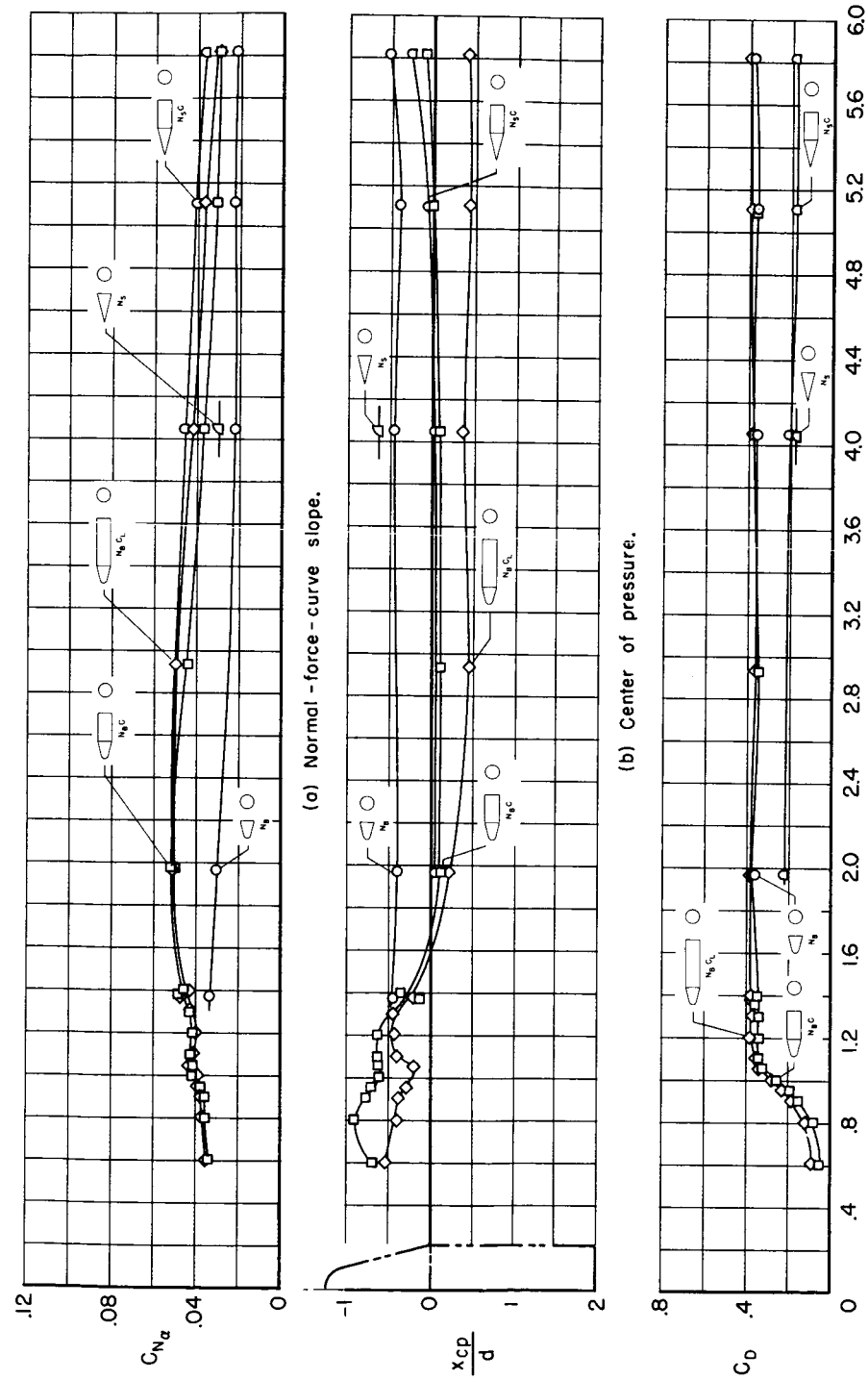


Figure 3.- Effect of nose bluntness and body length on aerodynamic characteristics of bodies; $\alpha = 0^\circ$.

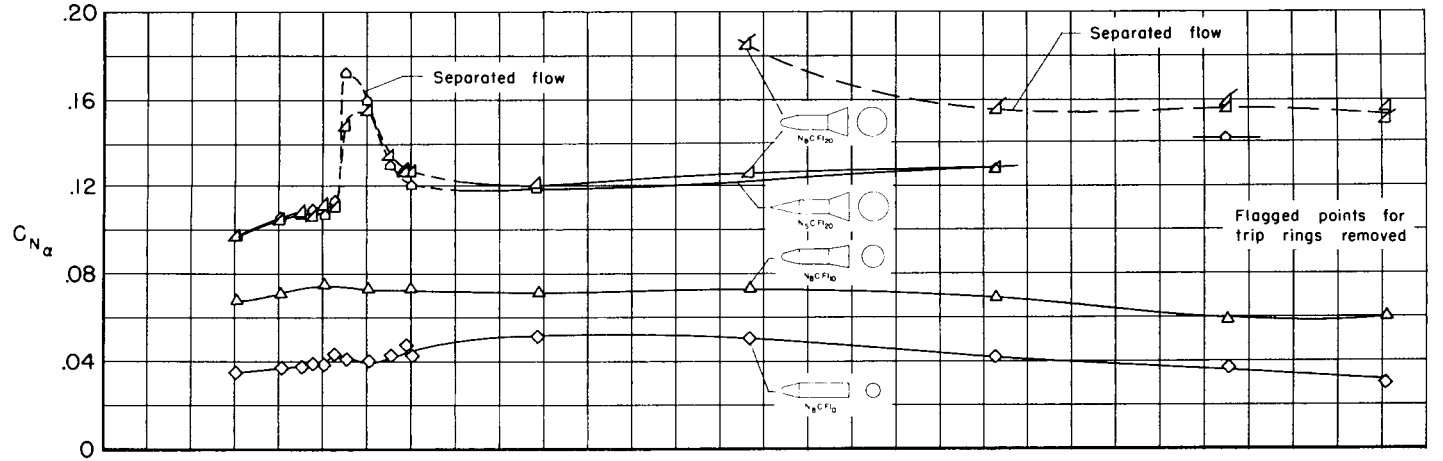


(a) Normal-force-curve slope.

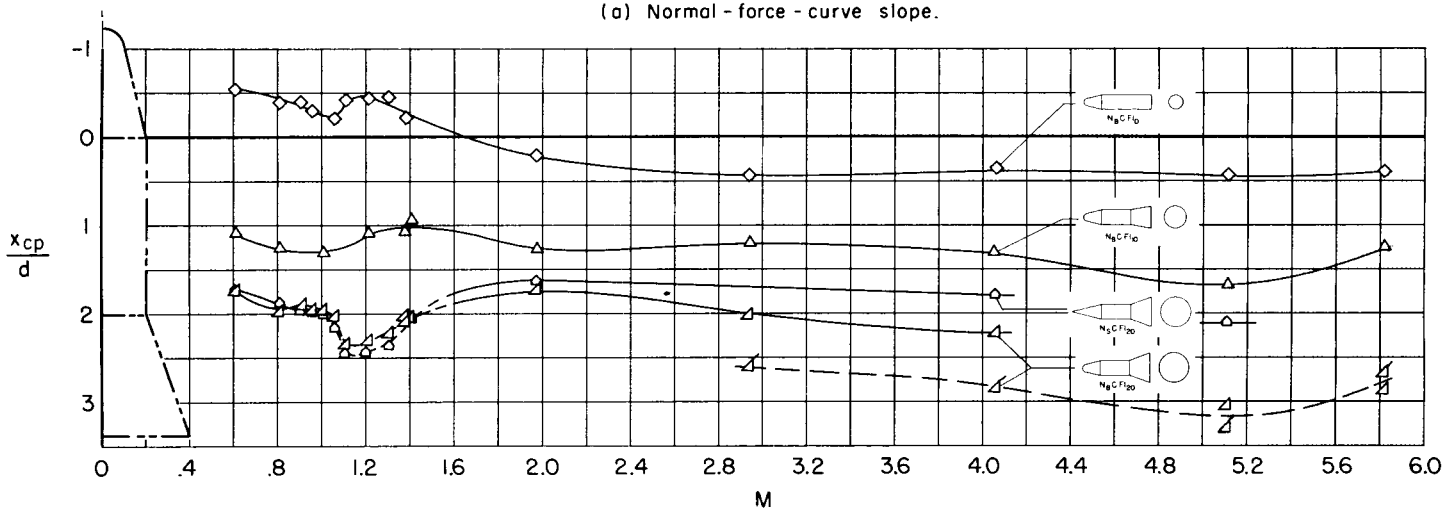


(b) Center of pressure.

Figure 4.- Effect of flare angle on aerodynamic characteristics of flared bodies; $\alpha = 0^\circ$.

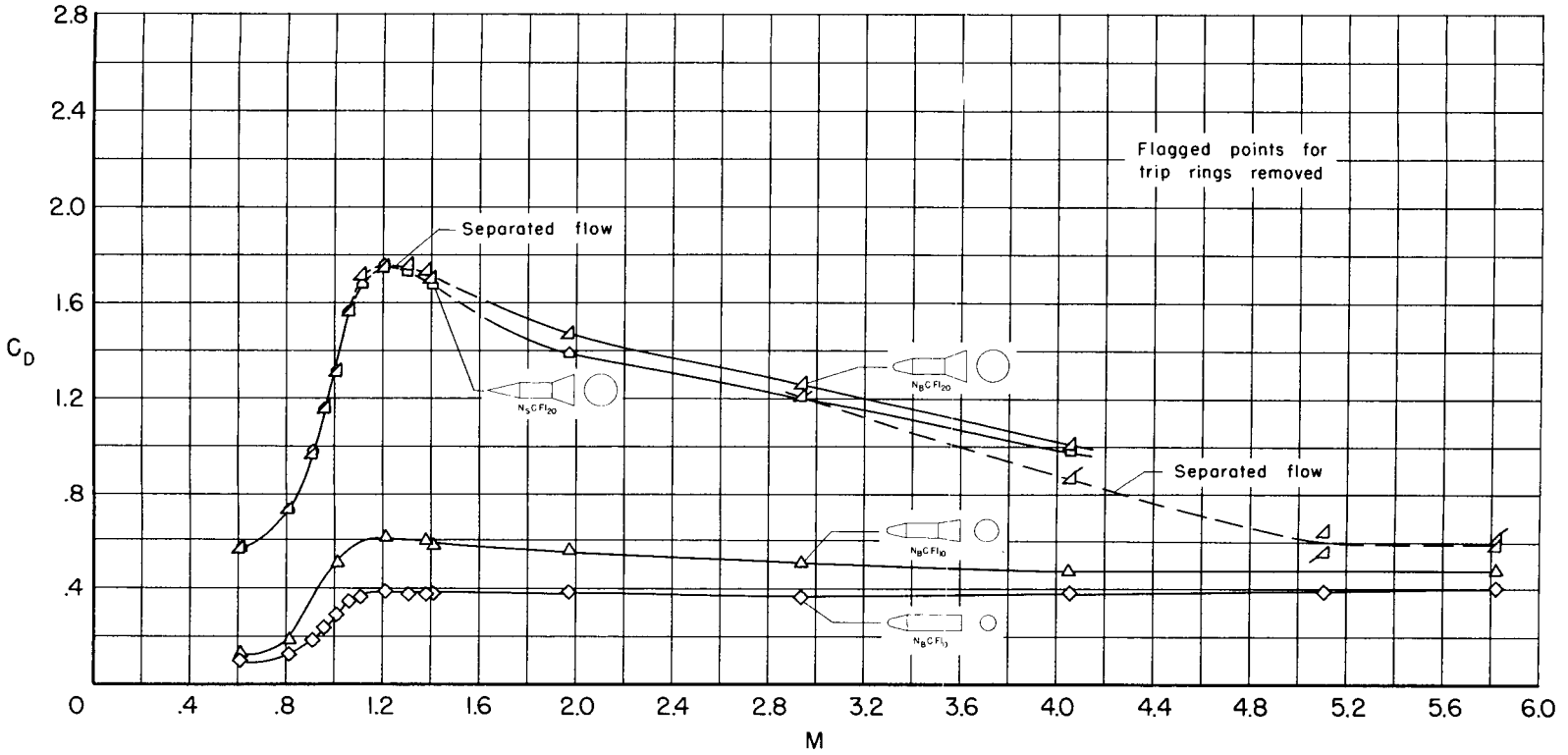


(c) Drag.

Figure 4.- Concluded.

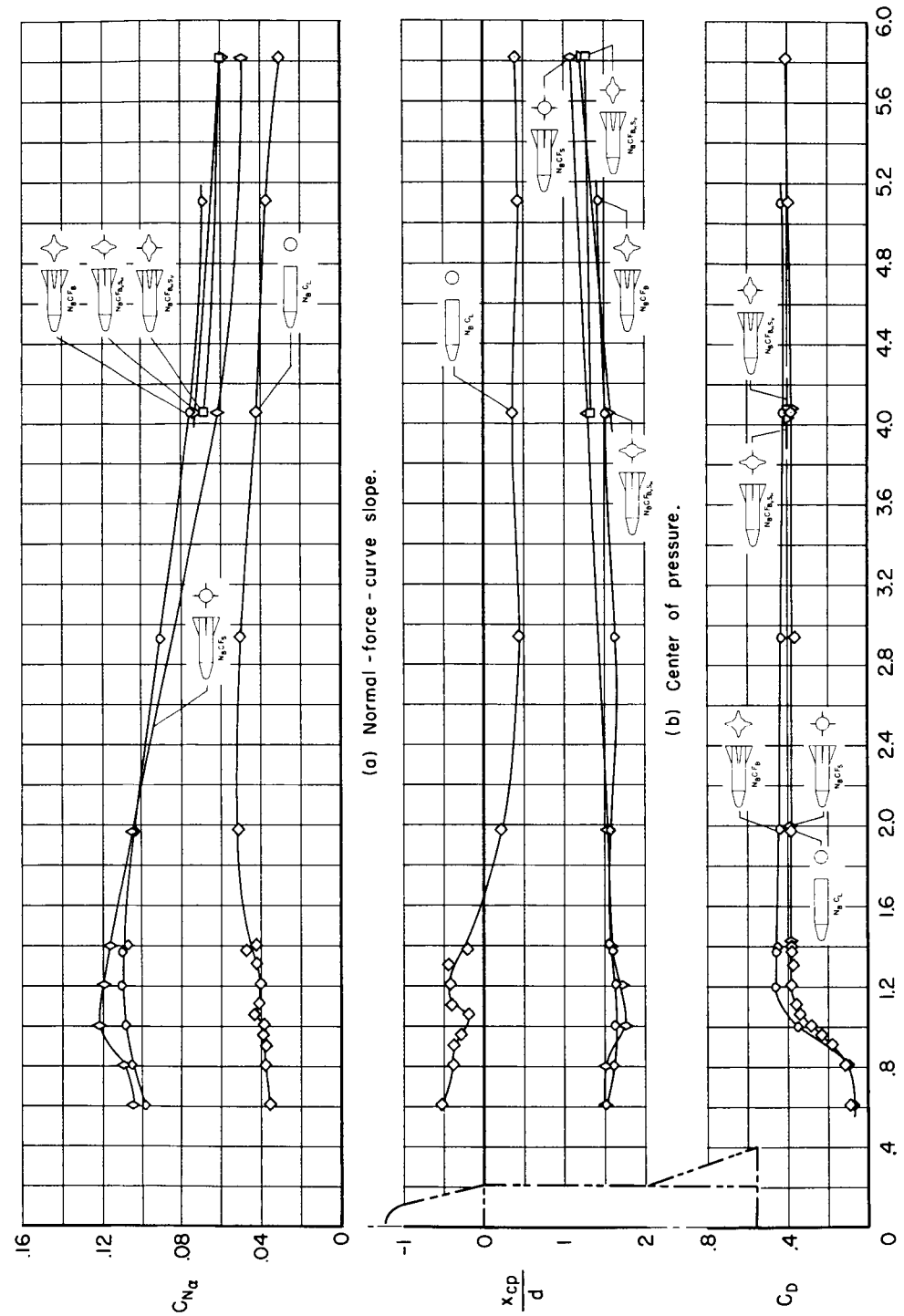


Figure 5.- Effect of fin bluntness on aerodynamic characteristics of finned bodies; $\alpha = 0°$.

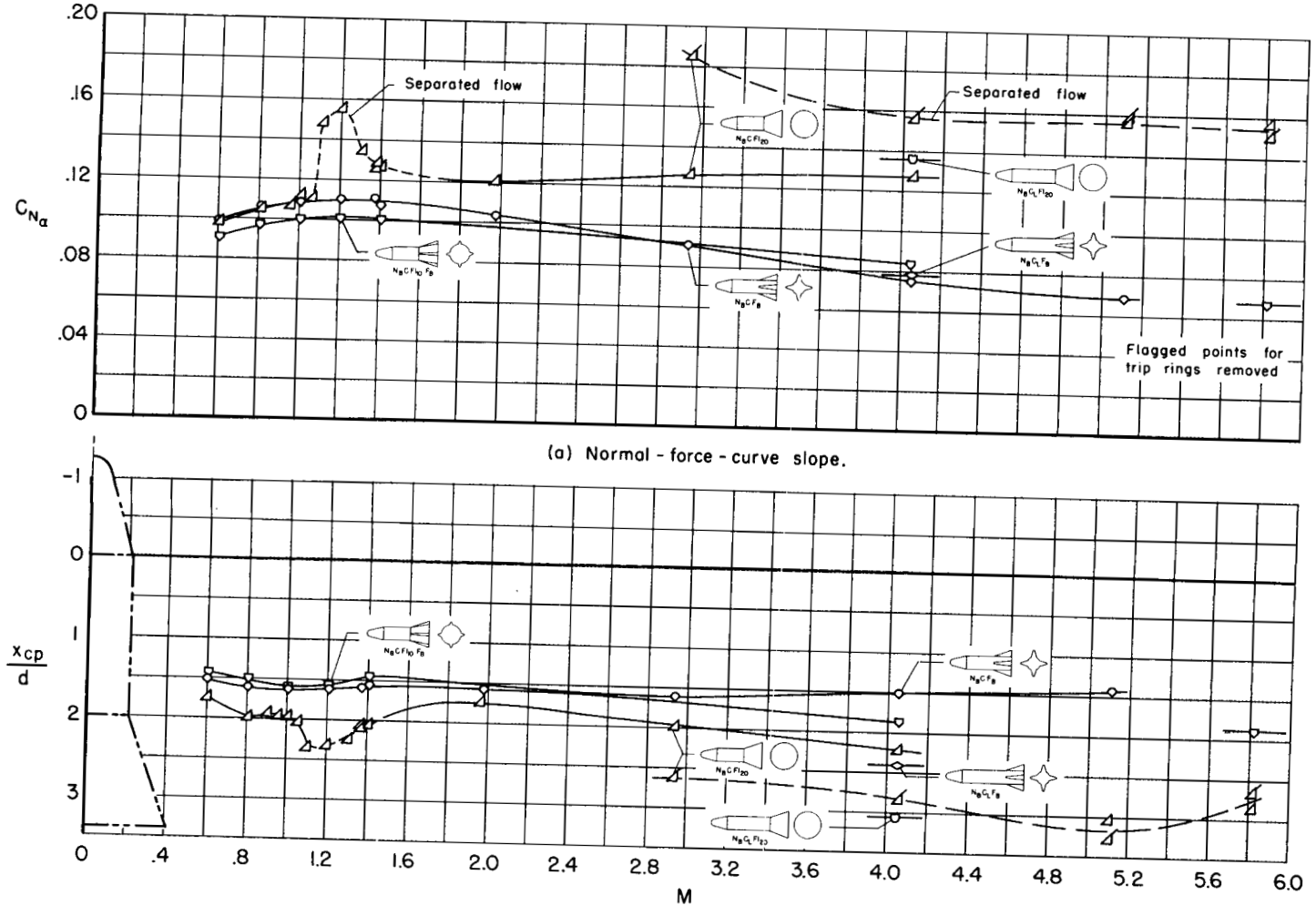


Figure 6.- Comparison of aerodynamic characteristics of flared and finned bodies of equal plan form; $\alpha = 0^{\circ}$.

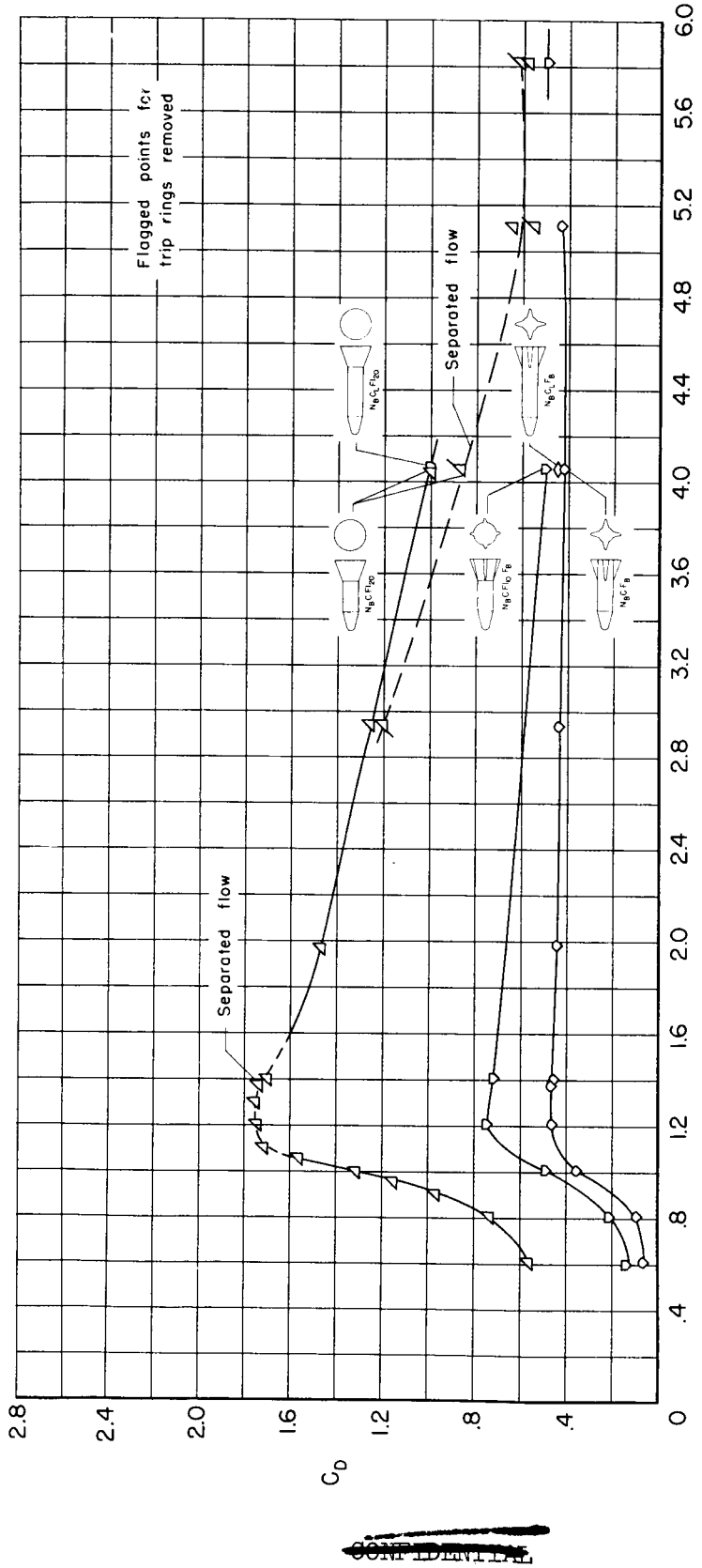


(c) Drag.

Figure 6.- Concluded.

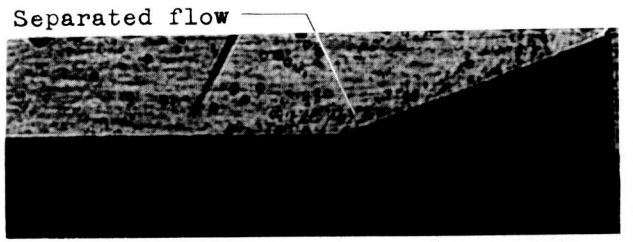


(a) M = 1.20; R = 0.38×10⁶; trip rings on nose.

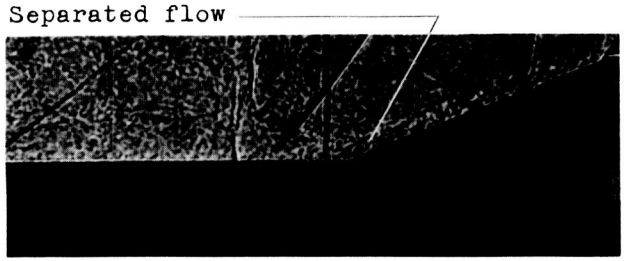


(b) M = 1.37; R = 0.38×10⁶; trip rings on nose.

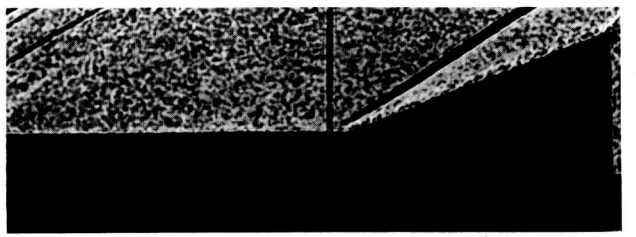

(c) M = 2.94; R = 0.49×10⁶; trip rings on nose.

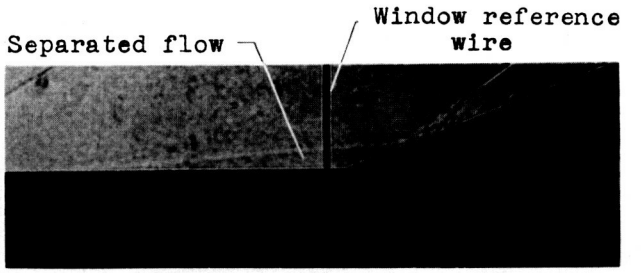


(d) M = 2.94; R = 0.49×10⁶; trip rings removed.

(e) M = 4.06; R = 0.49×10⁶; trip rings on nose.

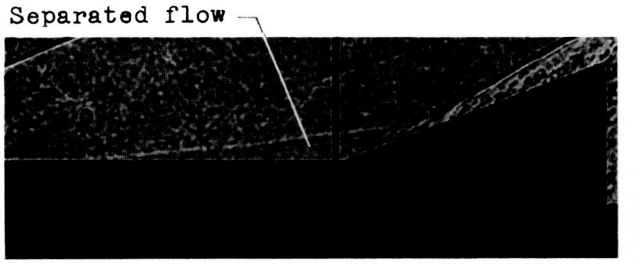


(f) M = 4.06; R = 0.49×10⁶; trip rings removed.

Figure 7.- Shadowgraphs of flow over afterbody of flared model $N_BCFl_{20}$; $\alpha = 0^o$.

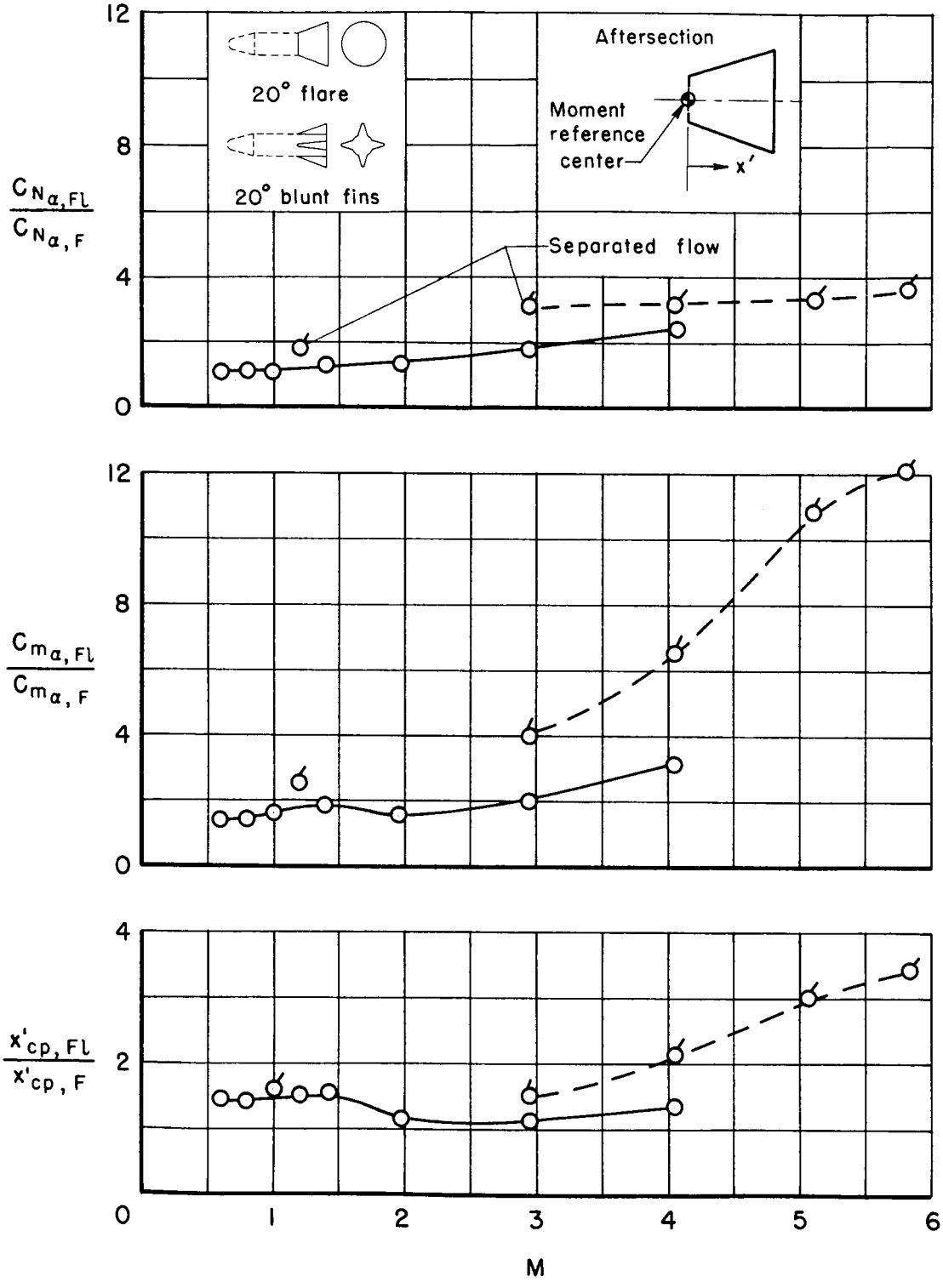


Figure 8.- Ratio of flare to fin effectiveness for equal plan-form area; $\alpha = 0^{\circ}$.

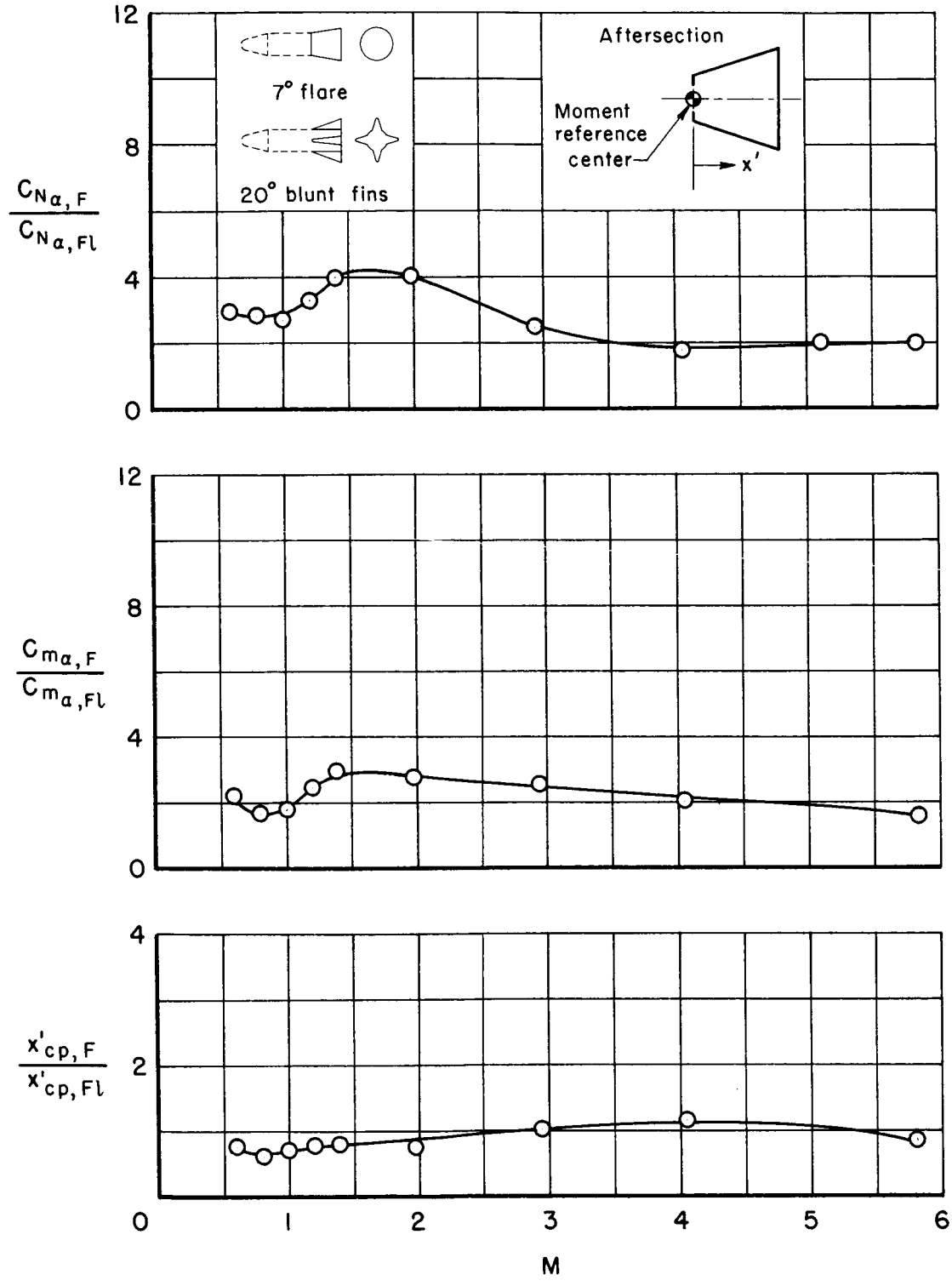


Figure 9.- Ratio of fin to flare effectiveness for equal drag; $\alpha = 0^{\circ}$.

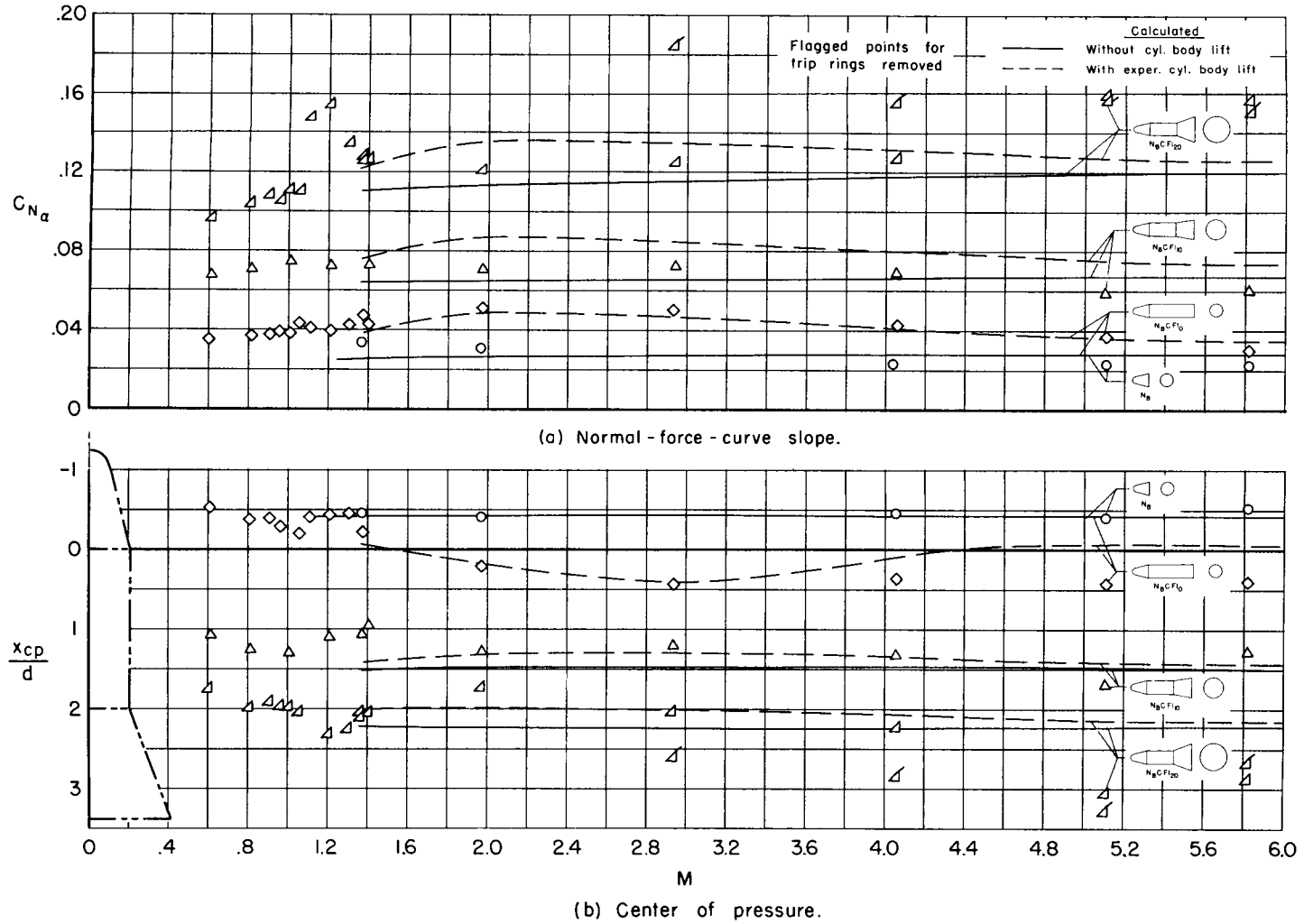


Figure 10.- Comparison of calculated results with experiment for flared bodies; $\alpha = 0^{\circ}$.

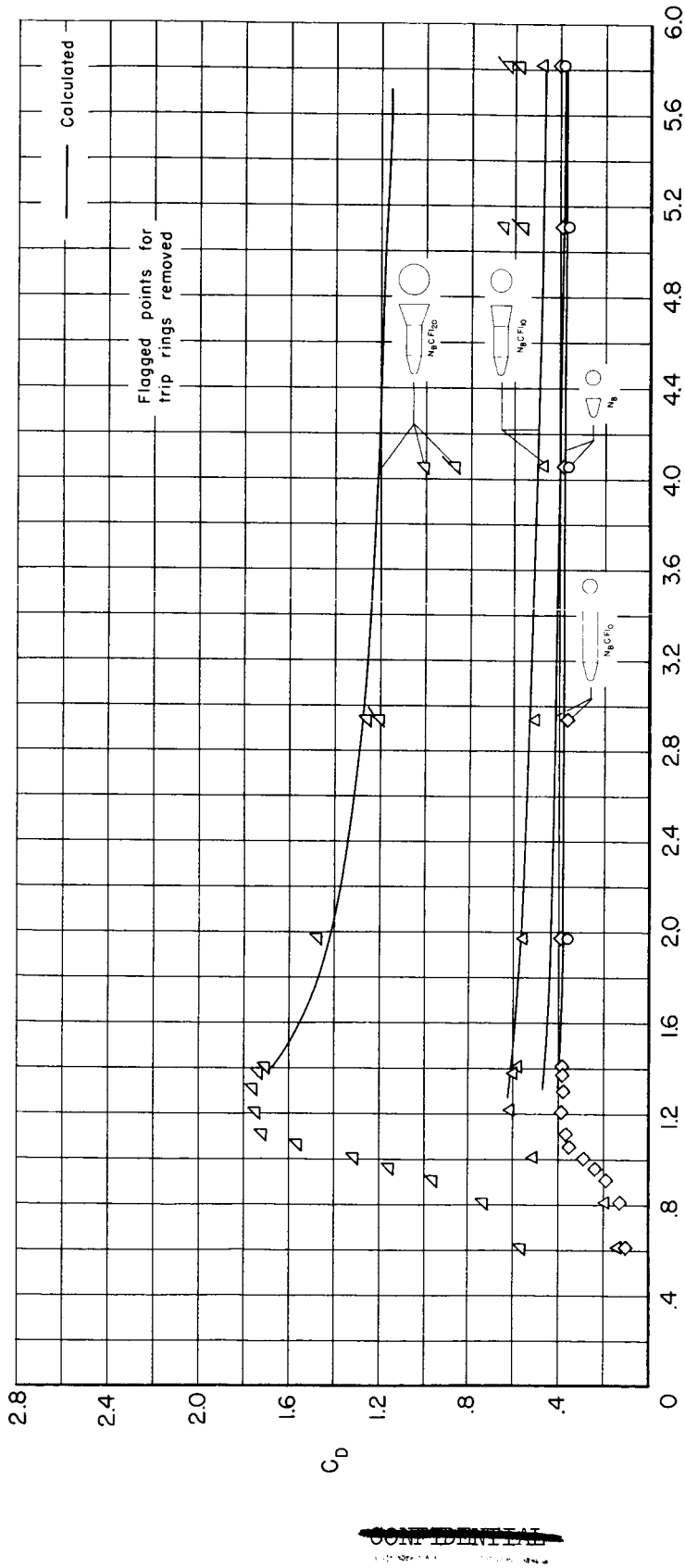


(c) Drag.

Figure 10.- Concluded.

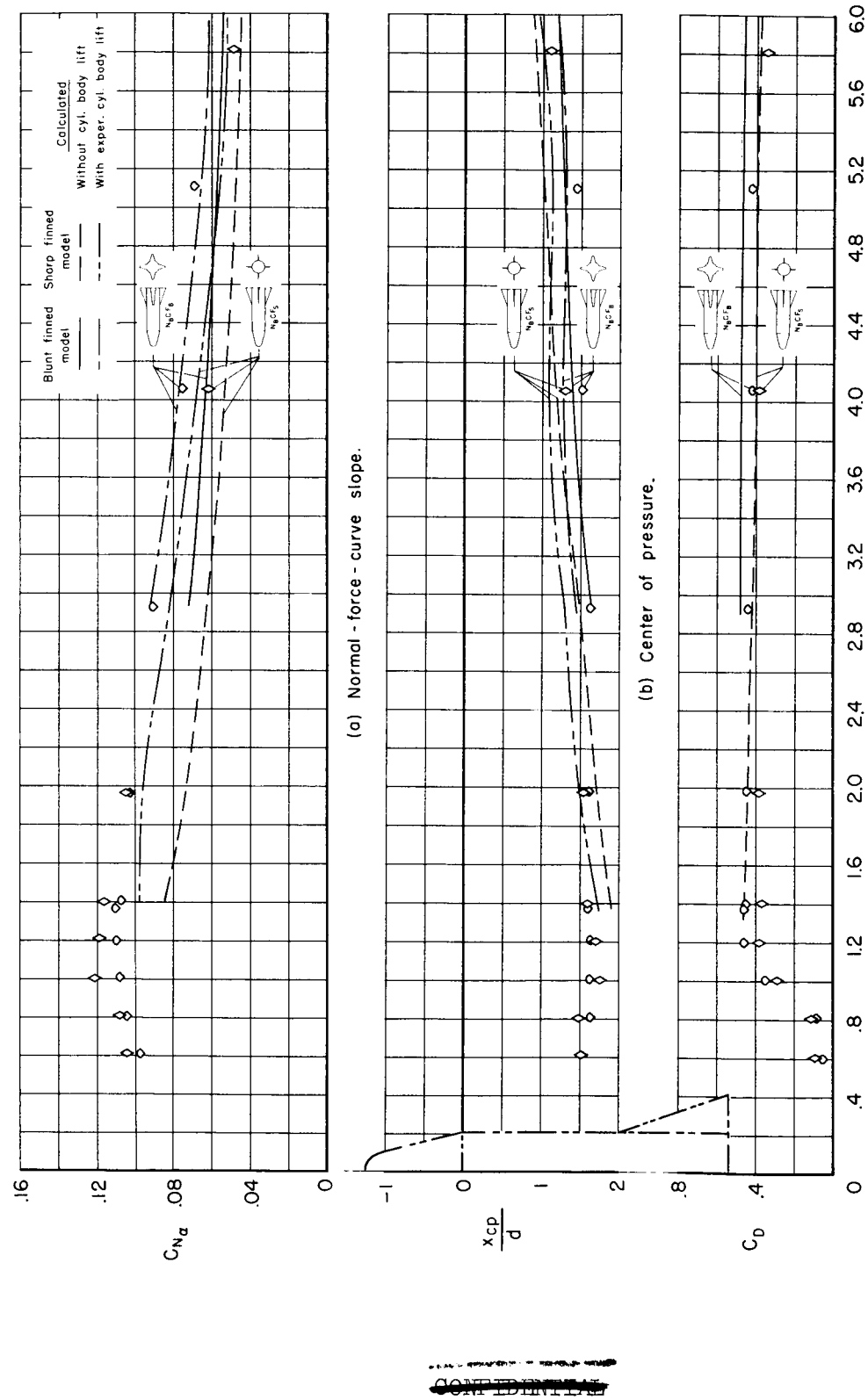


Figure 11.- Comparison of calculated results with experiment for finned bodies; $\alpha = 0^\circ$.

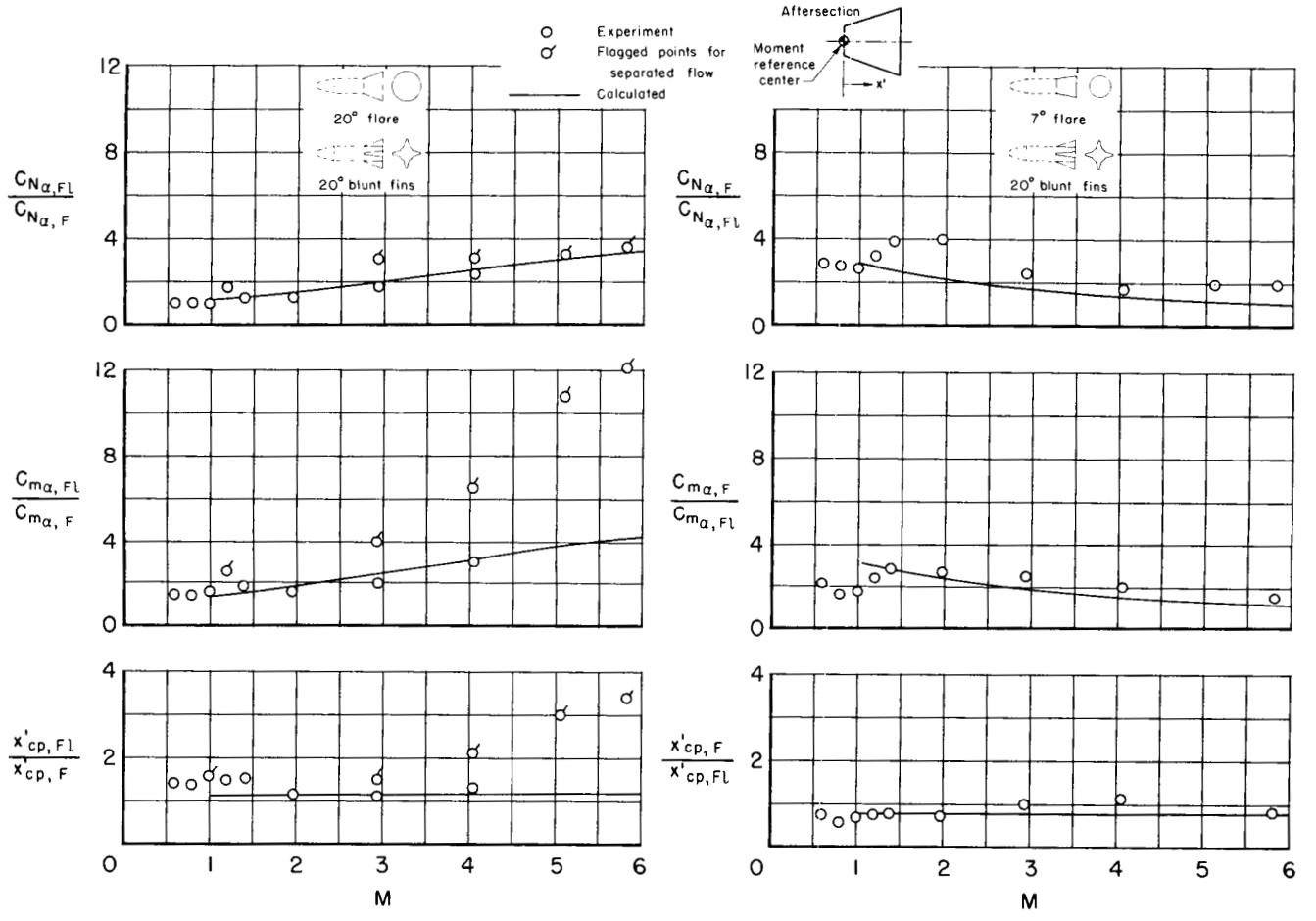


(a) Ratio of flare to fin effectiveness for equal plan-form area.

(b) Ratio of fin to flare effectiveness for equal drag.

Figure 12.- Comparisons of experiment with calculated results for relative effectiveness of flares and fins; $\alpha = 0^{\circ}$.